Eur. Phys. J. C (2025) 85:1349
https://doi.org/10.1140/epjc/s10052-025-15083-z

THE EUROPEAN PHYSICAL JOURNAL C

Regular Article - Theoretical Physics

Dynamics of quantum information resources in two-flavor neutrino oscillations

K. El Bouzaidi[1], **A. Slaoui**[2,1,a], **L. B. Drissi**[1,2,3], **E. H. Saidi**[1,2,3], **R. Ahl Laamara**[1,2]

[1] LPHE-Modeling and Simulation, Faculty of Sciences, Mohammed V University in Rabat, Rabat, Morocco
[2] Faculty of Sciences, Centre of Physics and Mathematics, CPM, Mohammed V University in Rabat, Rabat, Morocco
[3] College of Physical and Chemical Sciences, Hassan II Academy of Sciences and Technology, Rabat, Morocco

Received: 3 October 2025 / Accepted: 14 November 2025

Abstract The burgeoning intersection of particle physics and quantum information science unveils significant connections, particularly in the context of neutrinos–fundamental particles that challenge our understanding of mass, mixing, and coherence at the quantum level. This work investigates the quantum informational aspects of two-flavor neutrino oscillations, treating neutrino flavor change as a dynamic carrier of quantum resources in addition to a fundamental lepton physics phenomenon. Employing realistic experimental parameters from the Daya Bay, KamLAND, and MINOS experiments, we systematically evaluate four key quantum metrics: quantum coherence, entanglement, local quantum Fisher information (LQFI), and Bell non-locality. Our formalism utilizes time-dependent density matrices, incorporating environmental interactions modeled by a correlated dephasing channel to capture both Markovian (memoryless) and non-Markovian (memory-retaining) regimes. In the Markovian regime, coherence and LQFI exhibit exponential decay, with MINOS demonstrating the highest persistence of quantum features attributed to its long baseline (735 km) and high energy range (0.5–50 GeV). KamLAND, with a medium baseline and moderate energy, shows intermediate behavior, while Daya Bay's short baseline limits the survival of these quantum properties. Notably, Bell non-locality violation in the Markovian regime is exclusive to MINOS under high classical correlation strength, whereas Daya Bay and KamLAND remain within classical bounds. Across both regimes, particularly the non-Markovian where information backflow enhances coherence and entanglement, MINOS consistently emerges as the most robust setup for the preservation of quantum information.

1 Introduction

Neutrinos, often referred to as the "ghost particles" of the universe, are among the most enigmatic constituents of the Standard Model of particle physics. Despite possessing incredibly small masses and carrying no electric charge, neutrinos play a crucial role in shaping our understanding of the fundamental forces and components of the universe. These particles interact only via the weak nuclear force and gravity, rendering them nearly impervious to ordinary matter. As a result, trillions of neutrinos pass through our bodies every second–undetected and unimpeded–making their study a challenging yet highly rewarding pursuit in modern physics [1,2]. The phenomenon of neutrino oscillations, initially proposed by Bruno Pontecorvo, has fundamentally altered our comprehension of these particles. Oscillations occur when neutrinos, produced in specific flavor states (electron, muon, or tau), propagate as a quantum superposition of mass eigenstates. This behavior challenges the Standard Model's initial assumption that neutrinos are massless and offers strong evidence for the possibility of non-zero neutrino masses [3,4]. The underlying physics of neutrino oscillations depends on the interplay between mass-squared differences Δm^2, mixing angles, and energy baselines, all of which determine the probability of flavor transitions. These parameters, investigated through decades of experimental research, form the cornerstone of modern neutrino physics.

Experimental efforts such as those undertaken by Daya Bay, KamLAND, and MINOS have been pivotal in characterizing the parameters that govern neutrino oscillations. Each of these experiments targets distinct aspects of neutrino behavior, from short-baseline reactor antineutrino studies (Daya Bay), to medium-baseline reactor experiments (KamLAND), and long-baseline accelerator-based investi-

[a] e-mail: abdallah.slaoui@um5s.net.ma (corresponding author)

Published online: 24 November 2025

gations (MINOS). By leveraging their unique configurations, these experiments probe different oscillation regimes, enabling a comprehensive understanding of mixing angles, mass-squared differences, and flavor-transition probabilities [5–7]. The disappearance of electron antineutrinos released by nuclear reactors over brief baselines (364–1912 m) is the main focus of the Daya Bay experiment. Its accurate measurements of the effective mass-squared difference Δm^2_{ee} and the mixing angle θ_{13} have set a benchmark for understanding the smallest of the neutrino mixing angles [8]. KamLAND, by contrast, detects electron antineutrinos from multiple nuclear reactors at medium baselines (approximately 180 km). It played a crucial role in confirming solar neutrino oscillation parameters, particularly the mass-squared difference Δm^2_{12} and the mixing angle θ_{12} [6,9]. Finally, MINOS is a long-baseline experiment that investigates muon neutrino oscillations over a distance of 735 km. It has provided stringent constraints on Δm^2_{32} and the mixing angle θ_{23}, thereby deepening our understanding of atmospheric neutrino oscillations [7]. While the physics of neutrinos has traditionally focused on flavor transitions and mass hierarchy, recent advances have unveiled their potential to serve as natural laboratories for exploring quantum information concepts. Neutrino oscillations inherently exhibit quintessential quantum properties, including coherence, entanglement, and sensitivity to external perturbations. Investigating these properties provides deeper insights into the interplay between classical and quantum correlations and highlights the role of environmental decoherence in shaping quantum systems [10,11].

Characterizing the quantum behavior of systems in quantum information science relies on key metrics such as quantum coherence, entanglement, local quantum Fisher information (LQFI), and Bell non-locality. Quantum coherence, a fundamental property of quantum mechanics, quantifies a system's ability to maintain superposition states. In the context of neutrino oscillations, coherence reflects their oscillatory behavior as they transition between flavor states, offering insights into how environmental interactions affect these transitions and how classical correlations can help sustain quantum behavior [12]. Entanglement, a hallmark of quantum mechanics, describes the non-separable correlations within composite quantum systems. In two-flavor neutrino models, where flavor states are superpositions of mass eigenstates, such long-range correlations naturally arise, making neutrino systems excellent candidates for exploring the interplay between entanglement and environmental decoherence [13]. LQFI quantifies quantum correlations within a discord-like framework by measuring a system's sensitivity to external perturbations. In neutrino systems, LQFI is used to assess the degree of non-classical correlations and their susceptibility to environmental effects; high LQFI values indicate robust quantum correlations and a system's capacity to retain information despite decoherence [14,15]. Finally, Bell non-locality reveals the intrinsically non-classical nature of neutrino oscillations through violations of Bell inequalities. This property directly measures non-local quantum behavior in neutrino systems, demonstrating correlations that defy classical realism and potentially enabling applications in quantum communication and cryptography [16,17].

Decoherence plays a significant role in neutrino oscillations, particularly in environments where interactions with matter or radiation lead to a loss of quantum coherence. This study employs the correlated dephasing channel framework, which models environmental effects as classical correlations between successive interactions of the neutrino system. By analyzing the impact of decoherence on quantum metrics, we gain insights into how environmental factors influence the dynamics of neutrino systems [18]. The dynamics of neutrino oscillations are influenced by the Markovian or non-Markovian characteristics of the environment. In the Markovian regime, defined by brief environmental correlation times, the system's evolution is dictated by exponential decay, resulting in a rapid loss of coherence. In contrast, the non-Markovian regime introduces memory effects, which manifest as oscillatory dynamics. Together, these two regimes capture a broad spectrum of environmental influences, allowing for a comprehensive analysis of quantum behavior in neutrino systems [19,20].

In this work, we consider a two-flavor neutrino model subjected to a classically correlated dephasing channel, which introduces classical correlations between successive interactions within the system [21]. This dephasing channel serves as a framework for modeling environmental effects. Through this lens, we explore how neutrino systems maintain quantum properties in both Markovian and non-Markovian regimes [19]. By incorporating experimental parameters from Daya Bay, KamLAND, and MINOS, we analyze the influence of mass-squared differences, mixing angles, and baselines on the quantum information metrics of neutrino systems. Our results highlight the nuanced interplay between environmental decoherence and neutrino oscillations, offering a fresh perspective on the quantum behavior of these elusive particles.

2 Bipartition mapping in neutrino oscillations

Bipartite quantum systems, consisting of two subsystems A and B, embody key principles such as entanglement, coherence, and non-locality. These systems are mathematically described by the tensor product of their individual Hilbert spaces, $\mathcal{H}_A$ and $\mathcal{H}_B$, forming the composite space $\mathcal{H}_A \otimes \mathcal{H}_B$. The richness of bipartite systems lies in their ability to exhibit correlations that defy classical explanations [22]. The joint orthonormal basis for the bipartite system $\mathcal{H}_A \otimes \mathcal{H}_B$ is defined as [23]

$$\{|i\rangle_A \otimes |j\rangle_B = |i, j\rangle_{AB}\}_{i=0,j=0}^{d_A-1,d_B-1}, \tag{1}$$

and the general density matrix describing a quantum state of such a bipartite system in this basis is given by

$$\rho_{A,B} = \sum_{i,k=0}^{d_A-1} \sum_{j,l=0}^{d_B-1} \rho_{ij,kl} |i, j\rangle\langle k, l|, \tag{2}$$

where $\rho_{ij,kl}$ are the matrix elements in the joint basis.

For pure states, the density matrix elements simplify to $\rho_{ij,kl} = a_{ij}a_{kl}^*$, where a_{ij} are the coefficients of the state vector. To describe the quantum state of a subsystem, one traces out the other subsystem. For subsystem A, the reduced density matrix is

$$\rho_A = \sum_{i,k=0}^{d_A-1} \left(\sum_{j=0}^{d_B-1} \rho_{ij,kj} \right) |i\rangle_A\langle k| \equiv \sum_{i,k=0}^{d_A-1} \rho_{ik}^A |i\rangle_A\langle k|. \tag{3}$$

Neutrino flavor states (ν_e, ν_μ, ν_τ) are not direct eigenstates of mass but are quantum superpositions of the mass eigenstates (ν_1, ν_2, ν_3), linked by the neutrino mixing matrix. In the two-flavor approximation, this matrix is parameterized by a mixing angle θ and determines the oscillatory behavior of neutrinos. This behavior is influenced by physical parameters such as the mass-squared difference Δm^2, energy, and travel distance [3,4]. Consequently, neutrino oscillations make neutrinos a natural laboratory for studying bipartite quantum systems, where flavor states form one subsystem and mass eigenstates form another, enabling rigorous analysis using tools such as density matrices and reduced states.

In fact, the flavor states are expressed as linear superpositions of mass eigenstates $|\nu_i\rangle$ ($i = 1, 2$), governed by the neutrino mixing matrix;

$$|\nu_\alpha\rangle = \sum_{i=1}^{2} U_{\alpha i} |\nu_i\rangle, \tag{4}$$

where $U_{\alpha i}$ are elements of the mixing matrix parameterized by a single mixing angle θ. The oscillation probability for a neutrino transitioning from one flavor to another over a propagation distance x is given by:

$$P_{\nu_\alpha \to \nu_\beta}(x) = \sin^2(2\theta) \sin^2\left(\frac{\Delta m^2 x}{4E}\right), \tag{5}$$

where Δm^2, E and x are the mass-squared difference, neutrino energy, and propagation distance, respectively [13,23,24].

The neutrino's flavor state can be expressed as

$$|\nu_\alpha(t)\rangle = a_{\alpha\alpha}(t)|\nu_\alpha\rangle + a_{\alpha\beta}(t)|\nu_\beta\rangle, \tag{6}$$

where $a_{\alpha\alpha}(t)$ and $a_{\alpha\beta}(t)$ are the time-dependent probability amplitudes. Mapping these states into the composite two-qubit basis yield

$$|\nu_e\rangle = |\mu e\rangle, \quad |\nu_\mu\rangle = |e\mu\rangle, \tag{7}$$

resulting in the time-evolved state:

$$|\nu_e(t)\rangle = a_{ee}(t)|\mu e\rangle + a_{e\mu}(t)|e\mu\rangle. \tag{8}$$

The density matrix for the neutrino system in the specified basis $\{|ee\rangle, |e\mu\rangle, |\mu e\rangle, |\mu\mu\rangle\}$ is given by

$$\begin{aligned}\rho_{e,\mu}(t) = {} & |e\mu\rangle\langle e\mu||a_{e\mu}(t)|^2 + |\mu e\rangle\langle \mu e||a_{ee}(t)|^2 \\ & + |\mu e\rangle\langle e\mu|a_{ee}(t)a_{e\mu}^*(t) \\ & + |e\mu\rangle\langle \mu e|a_{e\mu}(t)a_{ee}^*(t),\end{aligned} \tag{9}$$

Here, the off-diagonal terms represent quantum coherence between the flavor states. In a correlated dephasing channel, classical correlations and decoherence are introduced via the parameter $\eta(t)$, leading to the modified density matrix [25]

$$\begin{aligned}\rho_{e,\mu}(t) = {} & |e\mu\rangle\langle e\mu||a_{e\mu}(t)|^2 + |\mu e\rangle\langle \mu e||a_{ee}(t)|^2 \\ & + |\mu e\rangle\langle e\mu|\eta(t)a_{ee}(t)a_{e\mu}^*(t) \\ & + |e\mu\rangle\langle \mu e|\eta(t)a_{e\mu}(t)a_{ee}^*(t),\end{aligned} \tag{10}$$

where $\eta(t) = f^2(t) + [1 - f^2(t)]\gamma$, and $f(t)$ is the dephasing function. In a completely correlated dephasing channel, where $\gamma = 1$, η equals 1. Thus, the density operator (10) will remain time-independent in this particular instance.

When employing a wave packet approach [26–28], the density matrix $\rho_\alpha(x, t)$ describing the evolution of a neutrino state depends on both position and time. This time-dependent density matrix, integrated over time to capture the system's evolution under a correlated dephasing channel, is expressed in terms of the elements $F_{\beta\gamma}^\alpha(x)$ as follows

$$\begin{aligned}\rho_{e\mu}(x) = {} & |e\mu\rangle\langle e\mu|F_{ee}^e(x) + |\mu e\rangle\langle e\mu|\eta(t)F_{e\mu}^e(x) \\ & + |e\mu\rangle\langle \mu e|\eta(t)F_{\mu e}^e(x) + |\mu e\rangle\langle \mu e|F_{\mu\mu}^e(x),\end{aligned} \tag{11}$$

where the elements $F_{\beta\gamma}^\alpha(x)$ are defined as

$$F_{\beta\gamma}^\alpha(x) = \sum_{k,j} U_{\alpha j}^* U_{\alpha k} f_{jk}(x) U_{\beta j} U_{\gamma k}^*. \tag{12}$$

Here, $U_{\alpha j}$ and $U_{\alpha k}$ are elements of the PMNS mixing matrix. The function $f_{jk}(x)$ represents the wave-packet overlap, encoding the quantum mechanical interference between different mass eigenstates. The elements of the density matrix

depend on the wave-packet overlap function $f_{jk}(x)$, given by

$$f_{jk}(x) = \exp\left(-i\frac{\Delta m_{jk}^2 x}{2E} - \left(\frac{\Delta m_{jk}^2 x}{4\sqrt{2}E^2\sigma_x}\right)^2\right). \tag{13}$$

which encapsulates the quantum mechanical interference between different mass eigenstates. This formalism emphasizes how the dynamics of the neutrino system are influenced by both quantum coherence and classical correlations.

The function $f(t)$, which is defined as follows, allows the parameter $\eta(t)$ to further integrate the Markovian or non-Markovian aspect of the system:

$$f(t) = \exp\left(-\frac{t}{2\tau}\right)\left[\cosh\left(\frac{vt}{2\tau}\right) + \frac{\sinh\left(\frac{vt}{2\tau}\right)}{v}\right]. \tag{14}$$

with $v = \sqrt{|1-16\tau^2|}$. Regarding the system's dynamics, the regime is classified as Markovian when $\tau < 1/4$, transitioning to a non-Markovian regime when $\tau > 1/4$, which reflects the increasing significance of memory effects.

We leverage experimental data and parameters from three prominent neutrino oscillation experiments; Daya Bay [29], KamLAND [9,30], and MINOS [31,32]. Each of these experiments provides unique insights into neutrino oscillation physics, focusing on distinct aspects of flavor transitions.

The Daya Bay experiment is a short-baseline reactor antineutrino disappearance study that investigates electron antineutrinos emitted by nuclear reactors at baselines ranging from 364 m to 1912 m. Operating within the energy range $E \in [1\,\text{MeV}, 8\,\text{MeV}]$, Daya Bay has played a crucial role in precisely measuring the smallest neutrino mixing angle, θ_{13}, and the effective mass-squared difference, $\Delta m_{ee}^2 = (2.42^{+0.10}_{-0.11}) \times 10^{-3}\,\text{eV}^2$. These results have significantly advanced our understanding of the subdominant mixing in neutrino oscillations [33]. In contrast, the KamLAND experiment, a medium-baseline reactor antineutrino disappearance study, examines electron antineutrinos originating from multiple nuclear reactors, with an effective baseline of approximately $L = 180\,\text{km}$. Operating in the energy range $E \in [2\,\text{MeV}, 10\,\text{MeV}]$, KamLAND confirmed critical parameters of solar neutrino oscillations, including the mass-squared difference $\Delta m_{12}^2 = 7.49 \times 10^{-5}\,\text{eV}^2$ and the mixing angle θ_{12}. This experiment was pivotal in resolving the solar neutrino problem and establishing the Large Mixing Angle (LMA) solution [34]. On the other hand, the MINOS experiment is a long-baseline, accelerator-based study of muon neutrino disappearance over a distance of $L = 735\,\text{km}$. Operating at significantly higher energies $E \in [0.5\,\text{GeV}, 50\,\text{GeV}]$, MINOS has provided stringent constraints on the atmospheric neutrino oscillation parameters, including $\Delta m_{32}^2 = (2.32^{+0.12}_{-0.08}) \times 10^{-3}\,\text{eV}^2$ and the mixing angle θ_{23}. Its findings have been instrumental in advancing our understanding of dominant mixing in atmospheric neutrino oscillations [35].

The measurement parameters from each experiment (Δm^2, mixing angles, baselines (L), and energy ranges (E)) serve as critical inputs for our analysis. While both Daya Bay and KamLAND focus on electron-antineutrino disappearance, they probe different oscillation regimes due to variations in baseline lengths and energy ranges. In contrast, MINOS examines muon-neutrino disappearance, offering complementary insights into neutrino oscillations at high energies and long baselines. These experimental parameters are summarized in Table 1. By incorporating these parameters into the two-flavor model, we systematically analyze the evolution of quantum criteria under both Markovian and non-Markovian regimes. This approach not only reveals the quantum informational features inherent to neutrino oscillations but also highlights how experimental configurations influence quantum behavior in these elusive systems.

The dynamics of quantum information properties reveals the profound impact of environmental interactions, including those modeled by a correlated dephasing channel where the introduction of classical correlations significantly affects the evolution of these quantum metrics. By analyzing data from the Daya Bay, KamLAND, and MINOS experiments, we explore how these metrics evolve in both Markovian and non-Markovian regimes, providing valuable insights into the interplay between quantum information and neutrino physics.

3 Pairwise quantum criteria in two-flavor neutrino oscillations

3.1 Quantum coherence

The simultaneous existence of several states in superposition is known as quantum coherence, and it is a fundamental characteristic of quantum systems [12]. This characteristic is vital for numerous quantum technologies, such as quantum computing and quantum cryptography, as it enables systems to exhibit interference effects, thereby facilitating precise regulation and control of their behavior. This property is also central to the oscillatory behavior of neutrinos, as coherence directly governs the flavor-transition probabilities. Despite its importance, coherence is highly susceptible to environmental interactions, which can lead to decoherence and the loss of quantum characteristics. Consequently, preserving coherence remains a critical challenge in the advancement of practical quantum technologies. Studying coherence in neutrino systems thus provides insight into how neutrino oscillations interact with their environment [36]. To quantify quantum coherence, several measures have been developed

Table 1 Summary of the key parameters for the Daya Bay, KamLAND, and MINOS experiments, including mass-squared differences, mixing angles, baselines, and energy ranges

Experiment	Oscillation parameters	Baseline and energy range
Daya Bay	$\Delta m^2_{ee} = (2.42^{+0.10}_{-0.11}) \times 10^{-3}\,\text{eV}^2$	$L = 364{-}1912\,\text{m},\ E = 1{-}8\,\text{MeV}$
	$\sin^2 2\theta_{13} = 0.084 \pm 0.005$	
KamLAND	$\Delta m^2_{12} = 7.49 \times 10^{-5}\,\text{eV}^2$	$L = 180\,\text{km},\ E = 2{-}10\,\text{MeV}$
	$\tan^2 2\theta_{12} = 0.47$	
MINOS	$\Delta m^2_{32} = (2.32^{+0.12}_{-0.08}) \times 10^{-3}\,\text{eV}^2$	$L = 735\,\text{km},\ E = 0.5{-}50\,\text{GeV}$
	$\sin^2 2\theta_{23} = 0.95 \pm 0.035$	

[37]; among these, the widely used l_1-norm of coherence is described as

$$C_{l_1}[\rho(t)] = \sum_{i \neq j} |\rho_{ij}(t)|, \tag{15}$$

where the off-diagonal components of the density matrix are represented by $\rho_{ij}(t)$. Equation (15) represents the l_1-norm coherence as the sum of absolute values for off-diagonal components in the selected basis [38,39]. The system state from Eq. (11) can be used to concisely represent the l_1-norm coherence as

$$C_{l_1}[\rho(t)] = 2\left(|\eta(t) F^e_{e\mu}(x)| + |\eta(t) F^e_{\mu e}(x)|\right). \tag{16}$$

The coherence dynamics of neutrino oscillations were analyzed using the l_1-norm, a measure that quantifies the degree of quantum superposition. Figure 1 presents these results across six graphs, capturing both Markovian and non-Markovian regimes for the Daya Bay, KamLAND, and MINOS experiments. Each graph provides insights into how experimental parameters, such as baseline distance L and energy range E, influence the preservation of coherence.

In the Markovian regime, depicted in panels (a)-(b)-(c), the coherence exhibits an exponential decay characteristic of systems without memory effects. For Daya Bay (Fig. 1a), the coherence does not exceed 0.3. This behavior is attributed to the experiment's short baseline $L \in [364\,\text{m}, 1912\,\text{m}]$ and relatively moderate energy range $E \in [1\,\text{MeV}, 8\,\text{MeV}]$, both of which limit the extent of quantum interference. KamLAND (Fig. 1b), with its significantly longer baseline $L = 180\,\text{km}$ and intermediate energy range $E \in [2\,\text{MeV}, 10\,\text{MeV}]$, achieves a higher coherence value exceeding 0.5, reflecting the enhanced quantum superposition facilitated by the experimental setup. Meanwhile, MINOS (Fig. 1c), with the longest baseline $L = 735\,\text{km}$ and the highest energy range $E \in [0.5\,\text{GeV}, 50\,\text{GeV}]$, shows coherence values approaching 1. This outcome underscores the strong preservation of quantum coherence in experiments with extended propagation distances and higher energy scales. Across all three experiments, an increase in the classical correlation parameter γ leads to a corresponding rise in coherence, emphasizing the critical role of $\eta(t)$ in sustaining quantum superposition states. In the non-Markovian regime, as illustrated in panels (d), (e), and (f), the coherence dynamics exhibit oscillatory decay due to memory effects. For Daya Bay (Fig. 1d), coherence remains below 0.3, which, while consistent with the Markovian regime, shows oscillations indicative of a feedback mechanism where temporarily lost information is partially recovered by the system. Similarly, KamLAND (Fig. 1e) demonstrates coherence exceeding 0.5, with its oscillatory nature reflecting the prolonged retention of quantum correlations enabled by non-Markovian channels. In MINOS (Fig. 1f), coherence approaches 1, mirroring Markovian behavior yet highlighting how memory effects further enhance coherence over time.

These results collectively reveal how environmental interactions, governed by Markovian or non-Markovian dynamics, interplay with experimental parameters to influence coherence in neutrino oscillations. The consistent increase in coherence with higher values of γ across all regimes and experiments reinforces the significance of the classical correlation parameter in preserving quantum properties. Furthermore, the oscillatory decay observed in non-Markovian systems emphasizes the role of memory effects in sustaining coherence, offering a richer perspective on the dynamics of neutrino systems under varying environmental influences.

3.2 Bipartite entanglement of formation

In this section, we explore bipartite entanglement in elementary particle physics. We'll demonstrate that the entanglement of a balanced superposition of two particle flavors can be expressed in terms of flavor oscillation transition probabilities, which can then be exploited for quantum information tasks. To do this, we derive explicit expressions for the entanglement of formation in a two-flavor neutrino system, using the density matrix $\rho_{e\mu}(x)$ while a correlated dephasing channel is present.

For a system prepared in a mixed state, a measure that satisfies the quantum entanglement requirements is the entan-

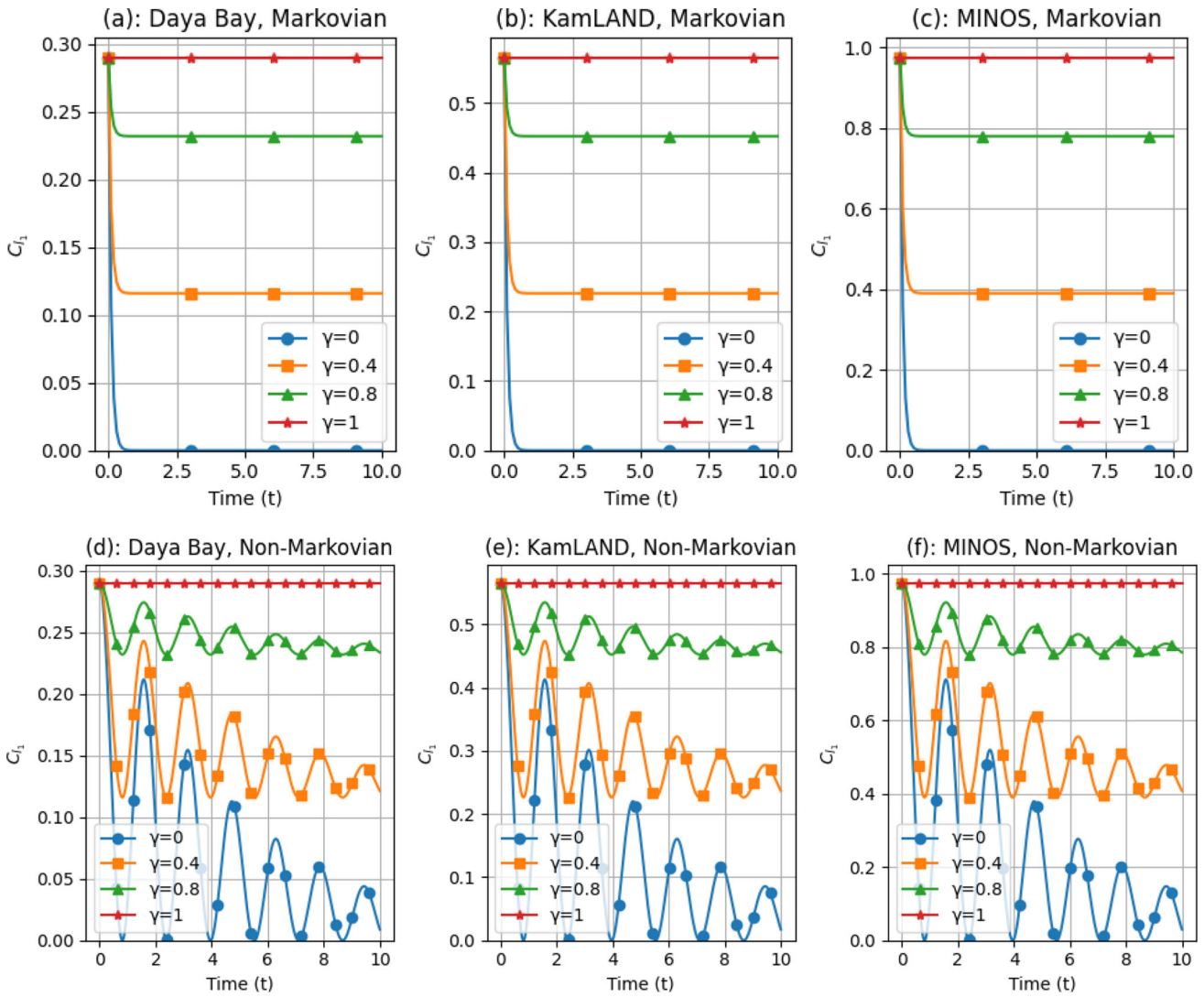

Fig. 1 Time dependence of quantum coherence in the Markovian regime with $\tau = 0.1$ and the non-Markovian regime with $\tau = 5$ for $4\omega = 2$, $T = 0.01$ and $\gamma = 0, 0.4, 0.8, and\ 1$, in Daya Bay, KamLAND and MINOS

glement of formation $E_F(\rho_{e\mu})$. It is defined as the minimal entanglement obtained over all pure state decompositions of a bipartite mixed state [40]. It is written

$$E_F(\rho_{e\mu}) = \min_{\{p_i, |\psi_i\rangle\}} \sum_i p_i E\left(|\psi_i\rangle\right), \tag{17}$$

where the minimization considers all possible pure spectral decompositions of the mixed state ρ. This entanglement quantifier is defined as the decomposition of a state that minimizes local entropies. For pure bipartite states, it corresponds directly to their local entropies. However, determining this measure analytically is difficult, as it requires considering all possible decompositions of a multipartite quantum state. Wootters [41] proposed a simple solution by giving an explicit formula for the formation of entanglement states of two qubits. It is expressed as

$$E_F(\rho_{e\mu}) = h\left(\frac{1+\sqrt{1-C(\rho_{e\mu})^2}}{2}\right), \tag{18}$$

where $h(x)$ is the binary entropy function $h(x) = -x\log_2(x) - (1-x)\log_2(1-x)$, and $C(\rho_{e\mu})$ is the Wootters concurrence defined mathematically as [42]

$$C(\rho_{e\mu}) = \max\left\{0, \sqrt{\vartheta_1} - \sqrt{\vartheta_2} - \sqrt{\vartheta_3} - \sqrt{\vartheta_4}\right\},$$

with the non-Hermitian operator $\rho_{e\mu}\tilde{\rho}_{e\mu}$ has eigenvalues ϑ_i that are arranged in descending order ($\vartheta_1 \geq \vartheta_2 \geq \vartheta_3 \geq \vartheta_4$). The spin-flipped density matrix $\tilde{\rho}_{e\mu}$ is defined as follows

$$\tilde{\rho}_{e\mu} = (\sigma_e^y \otimes \sigma_\mu^y)\rho_{e\mu}^*(\sigma_e^y \otimes \sigma_\mu^y),$$

where $\sigma_e^y = \sigma_\mu^y = \begin{pmatrix} 0 & -i \\ i & 0 \end{pmatrix}$ being the Pauli-y matrix. In our neutrino mixing matrix, the spin-flipped matrix is given by

$$\begin{aligned}\tilde{\rho}_{e\mu} = &|e\mu\rangle\langle e\mu| F^e_{\mu\mu}(x) + |\mu e\rangle\langle e\mu|\eta(t) F^e_{\mu e}(x) \\ &+ |e\mu\rangle\langle \mu e|\eta(t) F^e_{\mu e}(x) + |\mu e\rangle\langle \mu e| F^e_{ee}(x),\end{aligned} \tag{19}$$

and the eigenvalues of the operator $\rho_{e\mu}\tilde{\rho}_{e\mu}$ are

$$\begin{aligned}&\vartheta_1 = 4\left|\eta(t) F^e_{e\mu}(x)\right|^2, \quad \vartheta_2 = \left(F^e_{ee}(x) - F^e_{\mu\mu}(x)\right)^2, \\ &\vartheta_3 = 0, \quad \vartheta_4 = 0.\end{aligned} \tag{20}$$

Substituting these eigenvalues into the concurrence formula, we get

$$C(\rho_{e\mu}) = \max\{0, 2\left|\eta(t) F^e_{e\mu}(x)\right| - F^e_{ee}(x) - F^e_{\mu\mu}(x)\}. \tag{21}$$

The entanglement dynamics of neutrino oscillations, quantified by the entanglement of formation, reveal the complex interplay between environmental interactions and quantum correlations. The results are presented in two sets of panels: Fig. 2a–c correspond to the Markovian regime, while Fig. 2d–f illustrate the non-Markovian regime. These figures represent data from the Daya Bay, KamLAND, and MINOS experiments, respectively, providing comparative insights into the behavior of entanglement under different experimental configurations and environmental dynamics.

In the Markovian regime, entanglement exhibits a monotonic decay, a characteristic of systems dominated by memoryless environmental interactions. For the Daya Bay experiment (Fig. 2a), the entanglement of formation remains below 0.15. This limited entanglement can be attributed to the relatively short baseline ($L \in [364\,\text{m}, 1912\,\text{m}$) and moderate energy range ($E \in [1\,\text{MeV}, 8\,\text{MeV}$), which restrict the quantum interference effects essential for generating robust entanglement. KamLAND experiment (Fig. 2b), with its extended baseline ($L = 180\,\text{km}$) and intermediate energy range ($E \in [2\,\text{MeV}, 10\,\text{MeV}$), displays a higher entanglement value exceeding 0.3, reflecting the favorable conditions for stronger quantum correlations. In contrast, the MINOS experiment (Fig. 2c) is characterized by the longest baseline ($L = 735\,\text{km}$) and the highest energy range ($E \in [0.5\,\text{GeV}, 50\,\text{GeV}$). Here, the entanglement of formation approaches 1. This behavior underscores the enhanced preservation of entanglement in systems with longer propagation distances and higher energy scales. Across all three experiments, the classical correlation parameter γ exerts a significant influence, with higher values of γ leading to increased entanglement, highlighting the role of classical correlations in sustaining quantum properties.

The non-Markovian regime, shown in Panels 2d, 2e, and 2f, exhibits oscillatory entanglement dynamics. This behavior stems from the inherent feedback mechanism in non-Markovian systems, where information temporarily lost to the environment is partially retrieved. For the Daya Bay experiment (Panel 2d), entanglement stays below 0.15 but displays pronounced oscillations, which indicates recurring interactions with the environment. KamLAND (Panel 2e) shows a similar oscillatory pattern, with entanglement values exceeding 0.3, reflecting the prolonged retention of quantum correlations due to non-Markovian memory effects. The MINOS experiment (Panel 2f) achieves entanglement values close to 1, with oscillations amplifying the preservation of quantum correlations over time. These oscillations become especially prominent at higher values of γ, highlighting the combined role of non-Markovian dynamics and classical correlations in enhancing quantum entanglement.

Overall, these entanglement dynamics highlight the differing effects of Markovian and non-Markovian environments on quantum correlations in neutrino oscillations. The results show that memory effects in non-Markovian systems can not only preserve but also periodically revive entanglement, providing a deeper understanding of how neutrinos behave in different environmental settings. This analysis offers a comprehensive view of how experimental parameters and environmental regimes shape the quantum characteristics of neutrino oscillations, paving the way for further exploration of quantum phenomena in complex systems.

3.3 Metrological non-classical correlations in two-flavor neutrino oscillations

Recently, significant efforts have been made to establish the validity of quantum entanglement in quantum metrology. It has been shown that, in unitary processes, entanglement leads to a notable improvement in the accuracy of parameter estimation. Entanglement can even be exploited as a quantum resource to overcome the standard quantum limit and reach the Heisenberg limit [43–46]. This leads to a natural question: is it possible to relate and quantify quantum correlations in terms of quantum Fisher information? Several recent studies have explored this, with an important result being the introduction of a new measure of quantum correlations based on quantum Fisher information [47–50]. The LQFI has been introduced to deal with discord-like pairwise quantum correlations. This quantizer provides a better understanding of how quantum correlations contribute to the accuracy of quantum metrology. It also satisfies the key properties required for a good quantum correlation measure. It is also invariant under any local unitary operation and, for pure quantum states, it coincides with geometric discord. We will denote this measure by $\mathcal{F}(\rho_{AB})$, which corresponds to the optimal LQFI obtained using the measurement operator H_A, acting only on part A of the bipartite system AB [51]:

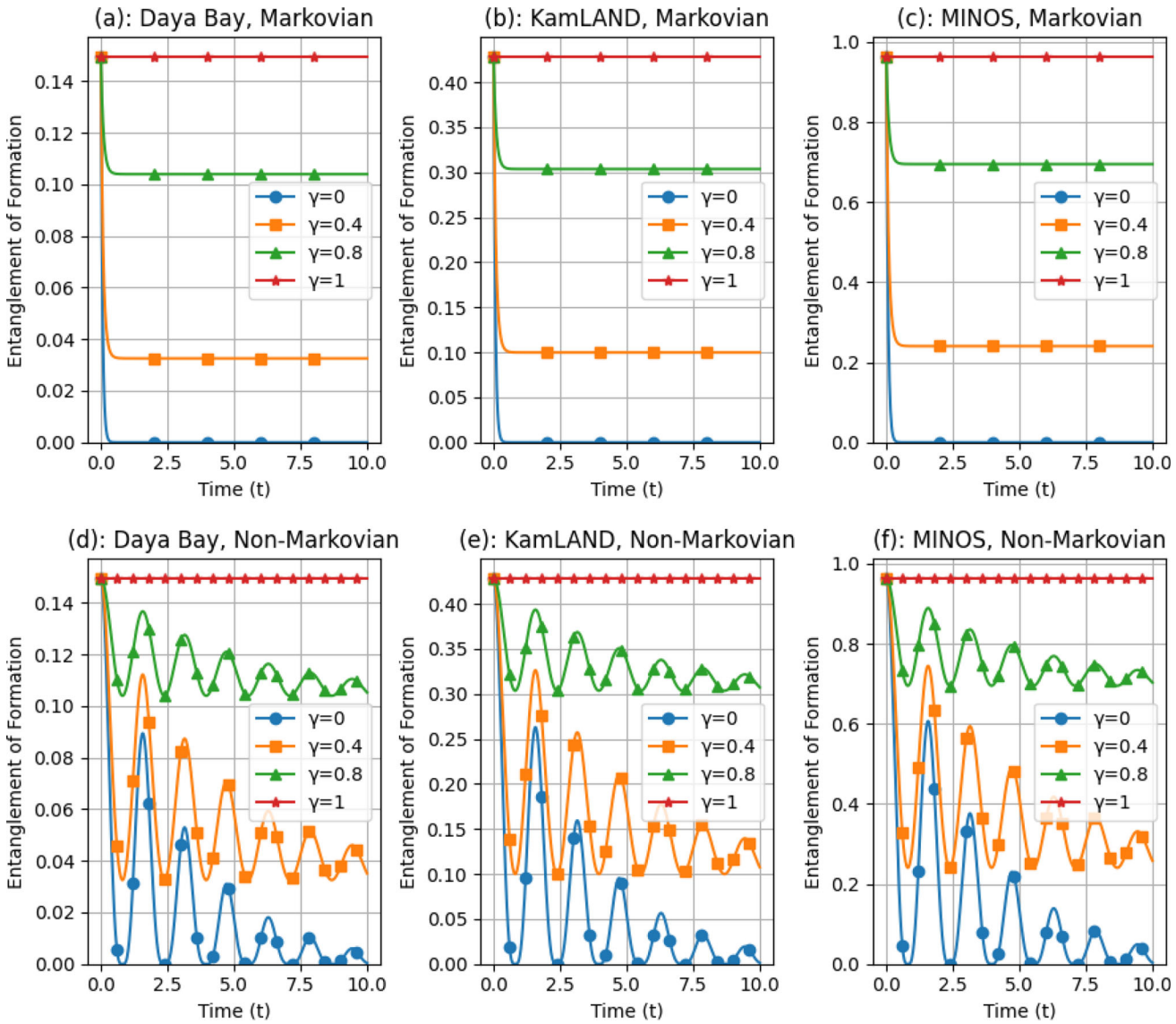

Fig. 2 Time dependence of entanglement of formation in the Markovian regime with $\tau = 0.1$ and the non-Markovian regime with $\tau = 5$ for $4\omega = 2$, $T = 0.01$ and $\gamma = 0, 0.4, 0.8$ and 1, in Daya Bay, KamLAND and MINOS

$$\mathcal{F}(\rho_{AB}) = \min_{H_A} F(\rho_{AB}, H_A), \tag{22}$$

with $F(\rho_{AB}, H)$ representing the QFI. It is remarkable that the authors [51] proved that the optimization defined by equation (22) is feasible, and that LQFI is

$$\mathcal{F}(\rho_{AB}) = 1 - \lambda_{\max}, \tag{23}$$

in the specific case where subsystem A is a qubit. In this case, $\lambda_{\max}$, the maximum eigenvalue of the symmetric matrix $\mathcal{M}$ representing the correlations between subsystems A and B, is computed as follows

$$\mathcal{M}_{\nu\mu} = \sum_{i,j} \frac{2q_i q_j}{q_i + q_j} \langle\psi_i|\sigma_\nu \otimes I|\psi_j\rangle\langle\psi_j|\sigma_\mu \otimes I|\psi_i\rangle, \tag{24}$$

where q_i are eigenvalues of $\rho_{A,B}(t)$, ψ_i are the corresponding eigenstates, and σ_ν, σ_μ denote the Pauli matrices in x, y, and z directions acting on the first qubit, I is the identity operator acting on the second qubit.

For the system considered, applying Eqs. (11) and (24) allows us to obtain the expressions of $\mathcal{F}_1 = 1 - \mathcal{M}_{zz}$, and $\mathcal{F}_2 = 1 - \mathcal{M}_{xx}$ in terms of the model parameters:

$$\mathcal{M}_{zz} = 1 - 4\eta^2(t)\left(|F^e_{ee}(x)|^2 + |F^e_{\mu\mu}(x)|^2\right), \tag{25}$$

where $\eta(t) = f^2(t)+[1-f^2(t)]\gamma$ accounts for the system's correlation parameter, and

$$\mathcal{M}_{xx} = 4\frac{\left(|\eta(t)F^e_{ee}(x)F^e_{e\mu}(x)|^2\right)\left(|F^e_{e\mu}(x)|^2+|F^e_{ee}(x)|^2\right)}{\left(1-\left(|F^e_{e\mu}(x)|^2-|F^e_{ee}(x)|^2\right)^2\right)^2}. \tag{26}$$

Accordingly, the LQFI can be expressed as

$$\mathcal{F}(\rho) = \min(\mathcal{F}_1, \mathcal{F}_2). \tag{27}$$

The LQFI, which quantifies the sensitivity of neutrino systems to parameter variations, provides critical insights into the interplay between quantum correlations and environmental influences. Figure 3 illustrates the LQFI dynamics across six panels, highlighting both the Markovian and non-Markovian regimes for Daya Bay, KamLAND, and MINOS. Each graph demonstrates how experimental configurations, such as baselines and energy ranges, affect the retention of quantum correlations.

In the Markovian regime, depicted in panels (a), (b), and (c) of Fig. 3, LQFI exhibits exponential decay consistent with the lack of memory effects. For Daya Bay (Fig. 3a), LQFI starts at 0 for $\gamma = 0$, indicating the absence of classical correlations, and rises to over 0.6 for $\gamma = 0.4$ and 1 for $\gamma = 1$. Notably, the results for $\gamma = 0.8$ are absent, suggesting that rapid decoherence suppresses LQFI for intermediate correlation values. This behavior reflects the relatively short baseline ($L \in [364\,\text{m}, 1912\,\text{m}]$) and moderate energy range ($E \in [1\,\text{MeV}, 8\,\text{MeV}]$), limiting the system's sensitivity to local perturbations. KamLAND (Fig. 3b), with its medium baseline ($L = 180\,\text{km}$) and broader energy range ($E \in [2\,\text{MeV}, 10\,\text{MeV}$), sustains LQFI across all values of γ, ranging from 0 for $\gamma = 0$ to over 0.8 for $\gamma = 0.8$. This behavior underscores the system's enhanced sensitivity to local measurements, facilitated by its experimental configuration. Conversely, MINOS (Fig. 3c) demonstrates significantly lower LQFI, with values peaking near 0.2 for $\gamma = 1$. The high energy range ($E \in [0.5\,\text{GeV}, 50\,\text{GeV}]$) and extended baseline ($L = 735\,\text{km}$) amplify decoherence, suppressing quantum correlations and diminishing sensitivity to local perturbations.

In the non-Markovian regime, illustrated in panels (d), (e), and (f) of Fig. 3, LQFI exhibits oscillatory decay patterns attributed to memory effects. For Daya Bay (Fig. 3d), while the overall trend remains consistent with the Markovian regime, the oscillations reflect the partial recovery of quantum correlations due to feedback from the environment. KamLAND (Fig. 3e) retains higher LQFI values with prominent oscillatory patterns, particularly for $\gamma \geq 0.4$, indicating that non-Markovian dynamics enhance sensitivity to parameter changes over time. MINOS (Fig. 3f), though exhibiting relatively lower LQFI, also displays oscillatory behavior, demonstrating that memory effects can partially counteract decoherence even in systems with long baselines and high energy ranges.

Overall, the results highlight the significant impact of experimental configurations on LQFI dynamics in neutrino systems. While the Markovian regime reveals the limitations imposed by short memory times, the non-Markovian regime underscores the advantages of memory effects in preserving quantum correlations. The increasing LQFI with higher γ across all regimes and experiments emphasizes the critical role of classical correlations in enhancing system sensitivity to local perturbations, offering valuable insights into the quantum behavior of neutrinos under various environmental conditions.

3.4 Bell non-locality in two-flavor neutrino oscillations

Bell non-locality describes a fundamental quantum phenomenon in which measurements on entangled particles reveal correlations that cannot be explained by classical physics. Introduced by John Bell, it probes the limits of classical realism through violations of Bell inequalities [17,52]. This phenomenon demonstrates that the behavior of these particles is intrinsically nonlocal and rules out the existence of local hidden variables. Neutrino systems, owing to the quantum superposition of their mass eigenstates and the entanglement of their flavor states, provide a unique testing ground for Bell non-locality. Violations of the Bell–CHSH inequality in such systems highlight their intrinsically quantum nature and reveal non-classical correlations that cannot be reproduced by local hidden variable theories [53]. For 2×2 quantum systems, the Bell–CHSH inequality serves as the primary tool to demonstrate the nonlocality of a state. The detection of this nonlocality relies on the violation of the inequality, which is defined as follows

$$|\langle\mathcal{B}_{\text{CHSH}}\rangle_\rho| \leq 2, \tag{28}$$

where $\langle\mathcal{B}_{\text{CHSH}}\rangle_\rho = \text{tr}(\rho\mathcal{B}_{\text{CHSH}})$ represents the expectation value of the Bell operator $\mathcal{B}_{\text{CHSH}}$ with respect to the quantum state ρ. The maximum possible violation of this inequality, known as the Bell parameter, is expressed as [54,55]:

$$\mathcal{B}_{\max}(\rho) = \max|\langle\mathcal{B}_{\text{CHSH}}\rangle_\rho| = 2\sqrt{\mathcal{N}(\rho)}. \tag{29}$$

Here, the quantity $\mathcal{N}(\rho)$ is computed from the eigenvalues ω_i ($i = 1, 2, 3$) of the matrix $\mathcal{X}^\dagger\mathcal{X}$, where $\mathcal{X}$ has elements $x_{\nu\mu} = \text{tr}(\rho\sigma_\nu \otimes \sigma_\mu)$ and $\sigma_{\nu,\mu}$ denote the Pauli matrices [56]. For the model under consideration, the matrix $\mathcal{N}(\rho)$ is given by

$$\mathcal{N}(\rho) = \max(\mathcal{N}_1, \mathcal{N}_2), \tag{30}$$

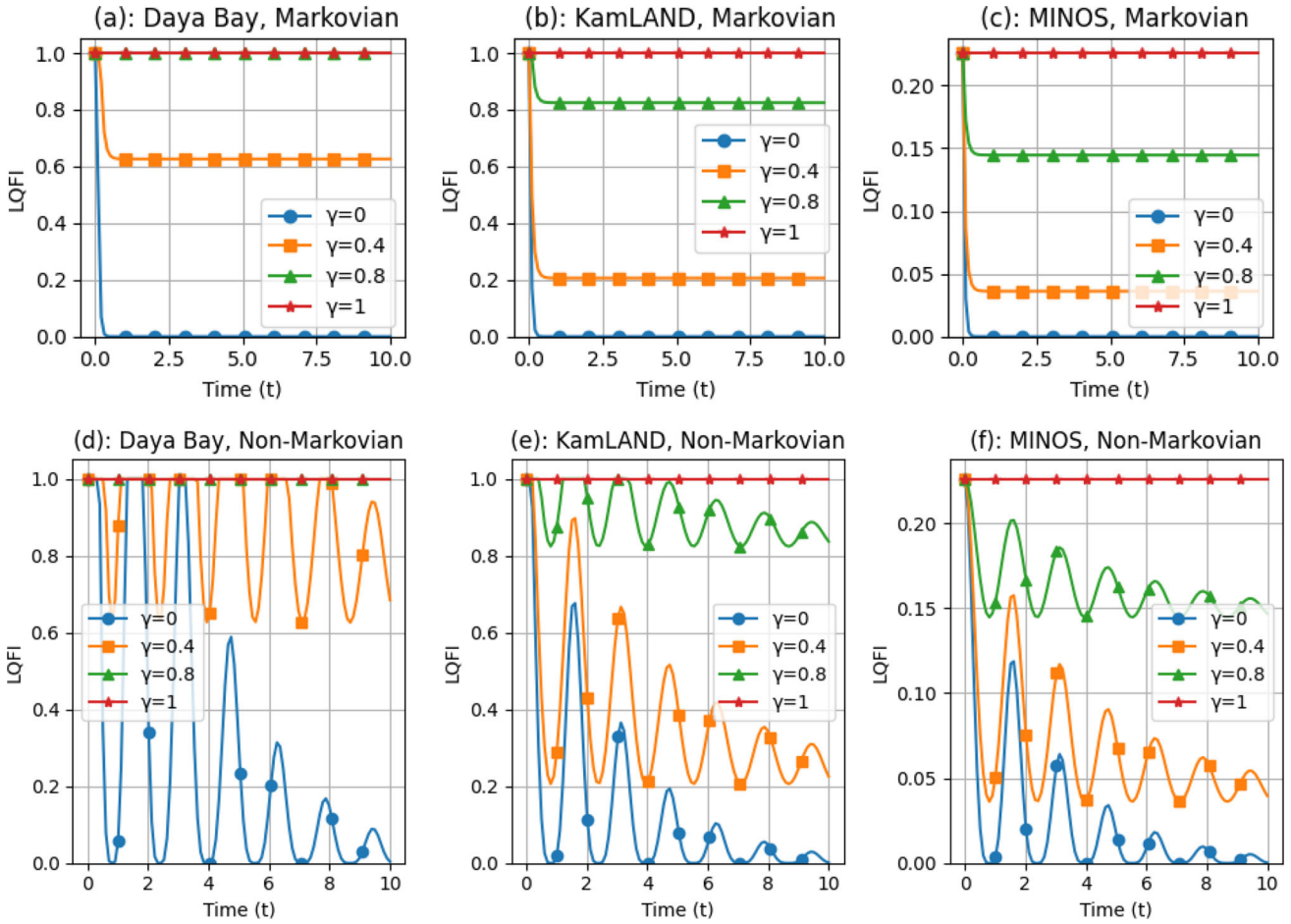

Fig. 3 Time dependence of LQFI in the Markovian regime with $\tau = 0.1$ and the non-Markovian regime with $\tau = 5$ for $4\omega = 2$ and $T = 0.01$. $\gamma = 0, 0.4, 0.8$ *and* 1 in Daya Bay, KamLAND and MINOS

where the quantity $\mathcal{N}_1$ captures the correlations arising from off-diagonal coherence terms

$$\mathcal{N}_1 = 8\left|\eta(t)F^e_{e\mu}(x)\right|^2. \tag{31}$$

with $F^e_{e\mu}(x)$ represents the wave-packet overlap for the off-diagonal terms, and the quantity $\mathcal{N}_2$ includes contributions from both diagonal and off-diagonal terms

$$\mathcal{N}_2 = 4\left|\eta(t)F^e_{e\mu}(x)\right|^2 + \left(F^e_{\mu\mu}(x) - F^e_{ee}(x)\right)^2, \tag{32}$$

where

$$\begin{aligned} F^e_{ee}(x) &= \sum_{k,j} U^*_{ej}U_{ek}f_{jk}(x)U_{ej}U^*_{ek}, \\ F^e_{\mu\mu}(x) &= \sum_{k,j} U^*_{\mu j}U_{\mu k}f_{jk}(x)U_{\mu j}U^*_{\mu k}. \end{aligned} \tag{33}$$

Violation of inequality (28) highlights the extent to which quantum correlations can exceed classical expectations, and is established if and only if the value of $\mathcal{N}(\rho)$ is greater than 1. Moreover, $\mathcal{N}(\rho)$ provides an effective measure for quantifying the degree of Bell non-locality in a bipartite state [57,58].

Bell non-locality, characterized by the Bell parameter $B_{\max}$, provides a critical metric for evaluating the extent to which neutrino systems exhibit correlations beyond classical realism. Figure 4 illustrates the dynamics of $B_{\max}$ for Daya Bay, KamLAND, and MINOS in both Markovian and non-Markovian regimes, with six panels labeled (a) through (f). These results reveal how baseline lengths, energy ranges, and the classical correlation parameter γ influence the manifestation of Bell non-locality in neutrino oscillations.

In the Markovian regime, shown in panels (a), (b), and (c) of Fig. 4, the behavior of $B_{\max}$ reflects the absence of memory effects, leading to exponential decay of quantum correlations. For Daya Bay (Fig. 4a), $B_{\max}$ remains entirely below the classical limit of $B_{\max} = 2$, regardless of the value of γ. This sub-classical behavior is consistent with the short baseline ($L \in [364\,\text{m}, 1912\,\text{m}]$) and moderate energy range ($E \in [1\,\text{MeV}, 8\,\text{MeV}]$), which limit the development

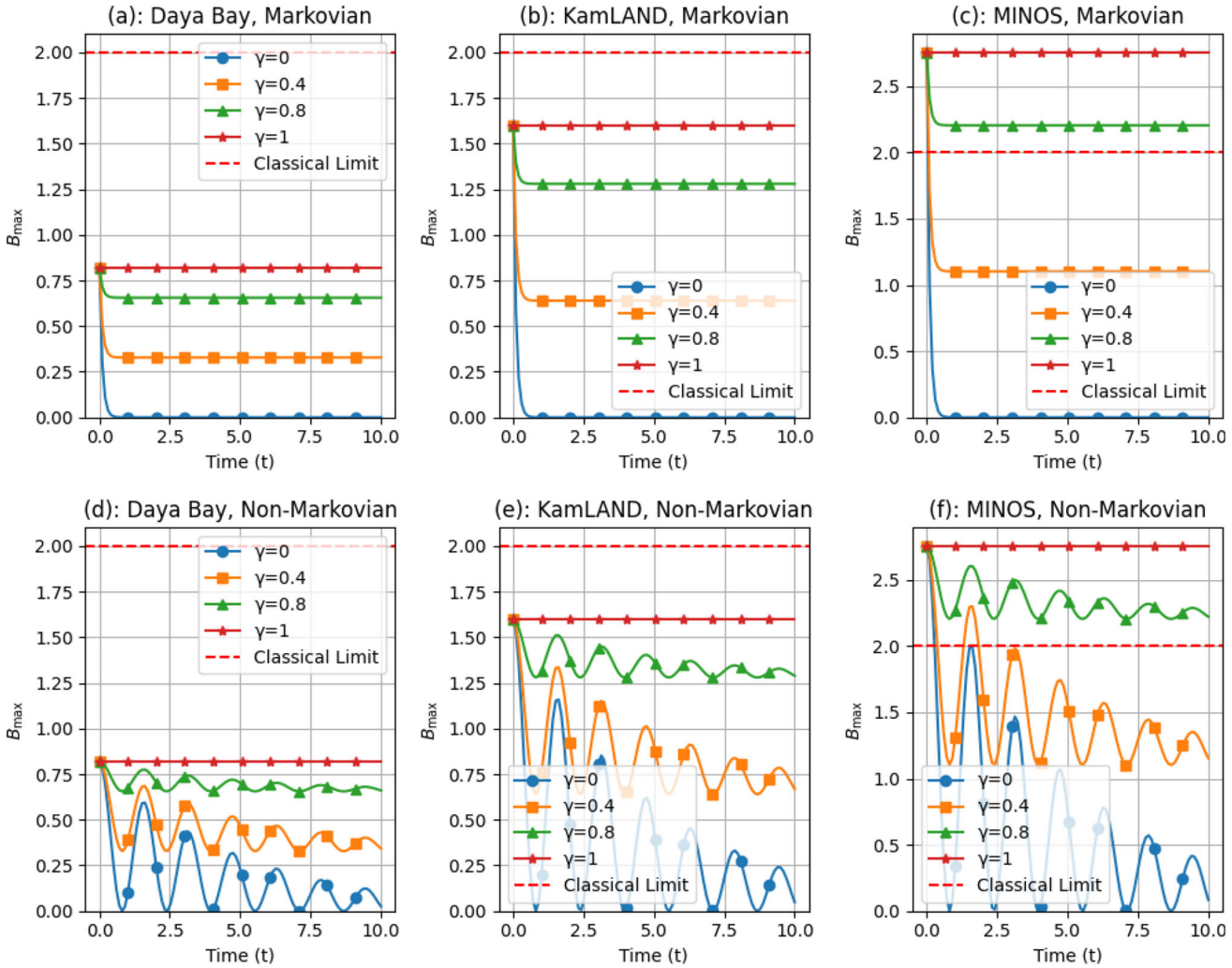

Fig. 4 Time dependence of Bell non locality in the Markovian regime with $\tau = 0.1$ and the non-Markovian regime with $\tau = 5$ for $4\omega = 2$ and $T = 0.01$. $\gamma = 0, 0.4, 0.8$ *and* 1 in Daya Bay, KamLAND and MINOS

of strong quantum correlations. KamLAND (Fig. 4b), with its longer baseline ($L = 180$ km) and intermediate energy range ($E \in [2\,\text{MeV}, 10\,\text{MeV}]$), approaches the classical limit for higher values of γ. Specifically, for $\gamma = 1$, $B_{\max}$ peaks around 1.5, indicating enhanced quantum correlations compared to Daya Bay. However, it remains within the classical limit, reflecting the system's sensitivity to the interplay between decoherence and baseline effects.

In contrast, MINOS (Fig. 4c) demonstrates a distinct transition from sub-classical to supra-classical behavior. For lower values of γ ($\gamma = 0$ and $\gamma = 0.4$), $B_{\max}$ remains below 2, consistent with classical correlations. However, for $\gamma = 0.8$ and $\gamma = 1$, $B_{\max}$ surpasses the classical limit, reaching nearly 3. This supra-classical behavior underscores the significant role of MINOS's long baseline ($L = 735$ km) and high energy range ($E \in [0.5\,\text{GeV}, 50\,\text{GeV}]$) in fostering robust quantum correlations, leading to observable non-locality.

The non-Markovian regime, depicted in panels (d), (e), and (f) of Fig. 4, introduces memory effects that manifest as oscillatory decay in $B_{\max}$. For Daya Bay (Fig. 4d), the sub-classical behavior persists, with $B_{\max}$ remaining below 2 for all values of γ. Similarly, KamLAND (Fig. 4e) retains its sub-classical nature, albeit with pronounced oscillations for higher γ, emphasizing the dynamic interplay between the neutrino system and the correlated dephasing channel. In MINOS (Fig. 4f), the non-Markovian regime preserves the supra-classical behavior observed for $\gamma = 0.8$ and $\gamma = 1$ in the Markovian case. The oscillatory patterns highlight the enhanced feedback of information between the environment and the system, sustaining strong quantum correlations over time. These results underscore the significant role of non-Markovian effects in amplifying Bell non-locality, particularly in systems with substantial classical correlations and favorable experimental configurations.

Overall, the analysis of $B_{\max}$ across different regimes and experiments demonstrates the profound influence of baselines, energy ranges, and classical correlations on the manifestation of Bell non-locality in neutrino systems. While Daya Bay and KamLAND predominantly exhibit sub-classical behavior, MINOS stands out as a platform for observing genuine quantum non-locality, particularly in the presence of non-Markovian dynamics. These findings provide a deeper understanding of how environmental interactions and experimental parameters shape the quantum nature of neutrino oscillations.

4 Conclusion

The investigation of quantum resources in two-flavor neutrino oscillations offers an unprecedented opportunity to bridge the gap between quantum information theory and particle physics. By analyzing coherence [12], entanglement [41], local quantum Fisher information [59], and Bell non-locality [52] within the framework of correlated dephasing channels [19], this work demonstrates how environmental interactions, baseline length, and neutrino energy shape the persistence of quantum correlations in open quantum systems. The comparative study of Daya Bay [5], KamLAND [6], and MINOS [7] experiments provides a concrete illustration of how physical configurations can amplify or suppress quantum features, offering valuable insight into the interplay between experimental design and quantum information dynamics. A central finding of this study is the sensitivity of quantum coherence and entanglement to the propagation conditions of neutrinos. The short baselines and moderate energies at Daya Bay constrain the degree of sustained quantum interference, resulting in limited preservation of coherence and lower entanglement values. KamLAND, operating at intermediate scales, reveals more robust quantum signatures, benefiting from extended propagation distances and broader energy ranges. MINOS, with its long baseline and high-energy spectrum, consistently demonstrates the most pronounced resilience across all quantum metrics. These variations underscore the crucial role of propagation length and energy in shaping the informational content of neutrino states.

The comparative analysis of Markovian and non-Markovian regimes further highlights the impact of environmental memory on quantum correlations. Markovian dynamics, dominated by irreversible information loss, impose exponential decay on coherence, entanglement, and sensitivity. In contrast, non-Markovian dynamics introduce oscillatory revivals, reflecting the backflow of information from the environment to the system [19]. This phenomenon is particularly pronounced for KamLAND and MINOS, where extended baselines enhance the role of memory effects, facilitating the periodic resurgence of entanglement and non-locality. These results emphasize the importance of including memory effects in realistic models of neutrino dynamics.

The role of classical correlations, represented by the parameter γ, emerges as a unifying theme across all metrics. Higher values of γ consistently enhance quantum coherence, extend the lifetime of entanglement, and amplify violations of the Bell inequality. This indicates that classical-quantum interplay can mitigate environmental decoherence, thereby sustaining quantum behavior. The analysis of LQFI provides an additional perspective by quantifying the parameter sensitivity of the system. While MINOS initially displays lower baseline sensitivity, its performance is significantly improved under strong classical correlations, highlighting the stabilizing role of γ in open quantum environments.

The evidence for Bell non-locality in neutrino oscillations is especially noteworthy. Violations of the Bell inequality in the MINOS configuration, even under Markovian conditions, establish neutrinos as a natural platform for probing nonlocal quantum correlations. In the non-Markovian regime, the persistence and oscillatory amplification of supra-classical behavior further illustrate the robustness of neutrino systems as testbeds for foundational questions in quantum mechanics. These findings position neutrino oscillations not merely as phenomena of particle physics [4] but as dynamic laboratories for exploring the principles of quantum information.

In summary, this work has established a unified framework for understanding how coherence, entanglement, sensitivity, and non-locality evolve in neutrino systems under environmental influences. The comparative analysis of experimental configurations reveals that long baselines and higher energies enhance quantum resources, while classical correlations and non-Markovian memory effects act as stabilizers against decoherence. These insights advance both the theoretical understanding of neutrino oscillations and their potential role in quantum information science. At the same time, this investigation opens the door to several pressing research directions. A natural extension concerns the inclusion of three-flavor dynamics, where the richer interference patterns may significantly reshape the evolution of coherence, entanglement, and non-locality under realistic experimental conditions. In astrophysical settings such as supernovae or the early universe, collective oscillations and matter effects [60] could either sustain or strongly suppress quantum resources, raising fundamental questions about their robustness in extreme environments. Another intriguing possibility is whether neutrino systems (owing to their extraordinarily weak interaction with matter) could be envisioned as carriers of quantum information across astrophysical distances. Furthermore, insights into the interplay between classical correlations and memory effects may guide the design of future neutrino experiments, optimizing their ability to probe quantum informational features. Finally, the parallels between neutrino oscillations in

correlated dephasing channels and noise-resilient protocols in quantum technologies suggest that lessons from neutrino physics might inspire new approaches for engineering robust quantum communication channels.

These questions outline a clear pathway for integrating neutrino physics with broader developments in quantum information theory and quantum technology. By pursuing these directions, future research can not only deepen our understanding of fundamental quantum behavior in neutrino systems, but also uncover novel opportunities for interdisciplinary applications at the interface of particle physics and quantum information science.

Funding No funding.

Data Availability Statement No data were used for the research described in the article. [Authors' comment: Data sharing not applicable to this article as no datasets were generated or analysed during the current study.]

Code Availability Statement Code/software will be made available on reasonable request. [Authors' comment: The code/software generated during and/or analysed during the current study is available from the corresponding author on reasonable request.]

Declarations

Conflict of interest The authors declare that they have no known competing financial interests or personal relationships that could have appeared to influence the work reported in this paper.

Funded by SCOAP[3].

References

1. Y. Fukuda, T. Hayakawa, E. Ichihara, K. Inoue, K. Ishihara, H. Ishino, Super-Kamiokande Collaboration, Evidence for oscillation of atmospheric neutrinos. Phys. Rev. Lett. **81**, 1562 (1998)
2. Particle Data Group, P. Zyla, R.M. Barnett, J. Beringer, O. Dahl, D.A. Dwyer, A. Pomarol, Review of particle physics. Prog. Theor. Exp. Phys. **2020**, 083C01 (2020)
3. S.M. Bilenky, Bruno Pontecorvo and neutrino oscillations. Adv. High Energy Phys. **2013**, 873236 (2013)
4. Z. Maki, M. Nakagawa, S. Sakata, Remarks on the unified model of elementary particles. Prog. Theor. Phys. **28**, 870–880 (1962)
5. F.P. An, J.Z. Bai, A.B. Balantekin, H.R. Band, D. Beavis, W. Beriguete, D. Mohapatra, Observation of electron-antineutrino disappearance at Daya Bay. Phys. Rev. Lett. **108**, 171803 (2012)
6. K. Eguchi, S. Enomoto, K. Furuno, J. Goldman, H. Hanada, H. Ikeda (KamLAND Collaboration), First results from KamLAND: evidence for reactor antineutrino disappearance. Phys. Rev. Lett. **90**, 021802 (2003)
7. P. Adamson, I. Anghel, A. Aurisano, G. Barr, M. Bishai, A. Blake (MINOS Collaboration), Phys. Rev. Lett. **112**, 191801 (2014)
8. K. Lau, (No. DOE-HOUSTON-41518). Univ. of Houston, TX (United States) (2014)
9. A. Gando, Y. Gando, H. Hanakago, H. Ikeda, K. Inoue, K. Ishidoshiro (KamLAND Collaboration), Reactor on-off antineutrino measurement with KamLAND. Phys. Rev. D **88**, 033001 (2013)
10. A. Streltsov, S. Rana, P. Boes, J. Eisert, Structure of the resource theory of quantum coherence. Phys. Rev. Lett. **119**, 140402 (2017)
11. S.F. Huelga, A. Rivas, M.B. Plenio, Non-Markovianity-assisted steady state entanglement. Phys. Rev. Lett. **108**, 160402 (2012)
12. T. Baumgratz, M. Cramer, M.B. Plenio, Quantifying coherence. Phys. Rev. Lett. **113**, 140401 (2014)
13. M. Blasone, F. Dell'Anno, S. De Siena, F. Illuminati, Entanglement in neutrino oscillations. Europhys. Lett. **85**, 50002 (2009)
14. S. Luo, Wigner–Yanase skew information vs. quantum Fisher information. Proc. Am. Math. Soc **132**, 885–890 (2004)
15. A. Slaoui, L. Bakmou, M. Daoud, R.A. Laamara, A comparative study of local quantum Fisher information and local quantum uncertainty in Heisenberg XY model. Phys. Lett. A **383**, 2241–2247 (2019)
16. A. Aspect, P. Grangier, G. Roger, Experimental tests of realistic local theories via Bell's theorem. Phys. Rev. Lett. **47**, 460 (1981)
17. J.S. Bell, On the Einstein Podolsky Rosen paradox. Phys. Phys. Fiz. **1**, 195 (1964)
18. G. Barenboim, A.M. Gago, Quantum decoherence effects: a complete treatment. Phys. Rev. D **110**, 095005 (2024)
19. H.P. Breuer, F. Petruccione, *The Theory of Open Quantum Systems* (OUP Oxford, Oxford, 2002)
20. I. González, Á. Rivas, Correlated and critical phenomena in multipartite quantum non-Markovianity. Phys. Rev. A **111**, L020204 (2025)
21. R.A. de Brito, B. de Lima Bernardo, Quantifying interference in multipartite quantum systems. Phys. Lett. A **384**, 126611 (2020)
22. M.A. Nielsen, I.L. Chuang, *Quantum Computation and Quantum Information* (Cambridge University Press, Cambridge, 2010)
23. V.A.S.V. Bittencourt, M. Blasone, S. De Siena, C. Matrella, Complete complementarity relations for quantum correlations in neutrino oscillations. Eur. Phys. J. C **82**, 1–6 (2022)
24. M. Blasone, F. Dell'Anno, S. De Siena, M. Di Mauro, F. Illuminati, Multipartite entangled states in particle mixing. Phys. Rev. D **77**, 096002 (2008)
25. S. Haddadi, M. Ghominejad, A. Czerwinski, Quantumness of gravitational cat states in correlated dephasing channels. Eur. Phys. J. C **84**, 670 (2024)
26. C. Giunti, Coherence and wave packets in neutrino oscillations. Found. Phys. Lett. **17**, 103–124 (2004)
27. C. Giunti, C.W. Kim, Coherence of neutrino oscillations in the wave packet approach. Phys. Rev. D **58**, 017301 (1998)
28. M. Blasone, F. Dell'Anno, S. De Siena, F. Illuminati, Flavor entanglement in neutrino oscillations in the wave packet description. Europhys. Lett. **112**, 20007 (2015)
29. Daya Bay Collaboration, Study of the wave packet treatment of neutrino oscillation at Daya Bay. Eur. Phys. J. C **77**, 606 (2017)
30. T. Araki, K. Eguchi, S. Enomoto, K. Furuno, K. Ichimura, H. Ikeda (KamLAND Collaboration), Measurement of neutrino oscillation with KamLAND: evidence of spectral distortion. Phys. Rev. Lett. **94**, 081801 (2005)
31. P. Adamson, C. Andreopoulos, K.E. Arms, R. Armstrong, D.J. Auty, D.S. Ayres, J.L. Thron, Measurement of neutrino oscillations with the MINOS detectors in the NuMI beam. Phys. Rev. Lett. **101**, 131802 (2008)

32. A.B. Sousa, MINOS and MINOS+ collaborations. in AIP Conf. Proc, vol. 1666, no. 110004 (2015), p. 35
33. D.M. Webber, Daya Bay Collaboration, An improved measurement of electron antineutrino disappearance at Daya Bay. Nucl. Phys. B **233**, 96–101 (2012)
34. S. Abe, T. Ebihara, S. Enomoto, K. Furuno, Y. Gando, K. Ichimura, KamLAND Collaboration, Precision measurement of neutrino oscillation parameters with KamLAND. Phys. Rev. Lett. **100**, 221803 (2008)
35. J.K. de Jong, MINOS Collaboration, Near-to-final MINOS oscillation results. Nucl. Phys. B **237**, 166–169 (2013)
36. J. Leggett, Qubits, cbits, decoherence, quantum measurement and environment. in *Fundamentals of Quantum Information: Quantum Computation, Communication, Decoherence and All That* (Springer Berlin Heidelberg, Berlin, Heidelberg, 2002), pp. 3–45
37. A. Streltsov, G. Adesso, M.B. Plenio, Colloquium: quantum coherence as a resource. Rev. Mod. Phys. **89**, 041003 (2017)
38. M.L. Hu, X. Hu, J. Wang, Y. Peng, Y.R. Zhang, H. Fan, Quantum coherence and geometric quantum discord. Phys. Rep. **762**, 1–100 (2018)
39. P. Pei, W. Wang, C. Li, H.S. Song, Using nonlocal coherence to quantify quantum correlation. Int. J. Theor. Phys. **51**, 3350–3358 (2012)
40. B.M. Terhal, K.G.H. Vollbrecht, Entanglement of formation for isotropic states. Phys. Rev. Lett. **85**, 2625 (2000)
41. W.K. Wootters, Entanglement of formation of an arbitrary state of two qubits. Phys. Rev. Lett. **80**, 2245 (1998)
42. A. Slaoui, B. Amghar, R. Ahl Laamara, Interferometric phase estimation and quantum resource dynamics in Bell coherent-state superpositions generated via a unitary beam splitter. J. Opt. Soc. Am. B **40**, 2013–2027 (2023)
43. F. Chapeau-Blondeau, Entanglement-assisted quantum parameter estimation from a noisy qubit pair: a Fisher information analysis. Phys. Lett. A **381**, 1369–1378 (2017)
44. V. Giovannetti, S. Lloyd, L. Maccone, Quantum-enhanced measurements: beating the standard quantum limit. Science **306**, 1330 (2004)
45. M. Abdellaoui, N.E. Abouelkhir, A. Slaoui, R.A. Laamara, Quantum phase estimation and realistic detection schemes in Mach–Zehnder interferometer using SU (2) coherent states. Phys. Lett. A **522**, 129786 (2024)
46. N. Abouelkhir, A. Slaoui, H. El Hadfi, R. Ahl Laamara, Estimating phase parameters of a three-level system interacting with two classical monochromatic fields in simultaneous and individual metrological strategies. J. Opt. Soc. Am. B **40**, 1599–1610 (2023)
47. L. Pezzé, A. Smerzi, Entanglement, nonlinear dynamics, and the Heisenberg limit. Phys. Rev. Lett. **102**, 100401 (2009)
48. A. Naimy, A. Slaoui, A. Ali, H. El Hadfi, R.A. Laamara, S. Al-Kuwari, Dynamic evolution of quantum Fisher and skew information under decoherence in three-qubit X-states. Phys. Lett. A **547**, 130536 (2025)
49. Á. Rivas, A. Luis, Precision quantum metrology and nonclassicality in linear and nonlinear detection schemes. Phys. Rev. Lett. **105**, 010403 (2010)
50. S. Gaidi, A. Slaoui, A.A. Mohamed, M.E. Falaki, R.A. Laamara, Effects of DM and KSEA interactions on entanglement, Fisher and Wigner–Yanase information correlations of two XYZ-Heisenberg-qubit states under a magnetic field. Phys. Scr. **99**, 115115 (2024)
51. D. Girolami, A.M. Souza, V. Giovannetti, T. Tufarelli, J.G. Filgueiras, R.S. Sarthour, G. Adesso, Quantum discord determines the interferometric power of quantum states. Phys. Rev. Lett. **112**, 210401 (2014)
52. N. Brunner, D. Cavalcanti, S. Pironio, V. Scarani, S. Wehner, Bell nonlocality. Rev. Mod. Phys. **86**, 419–478 (2014)
53. J.F. Clauser, M.A. Horne, A. Shimony, R.A. Holt, Proposed experiment to test local hidden-variable theories. Phys. Rev. Lett. **23**, 880 (1969)
54. M.L. Hu, Relations between entanglement, Bell-inequality violation and teleportation fidelity for the two-qubit X states. Quantum Inf. Process **12**, 229–236 (2013)
55. N. Zidan, A.U. Rahman, S. Haddadi, A. Czerwinski, S. Haseli, Local quantum uncertainty and quantum interferometric power in an anisotropic two-qubit system. Universe **9**, 5 (2022)
56. R. Horodecki, P. Horodecki, M. Horodecki, Violating Bell inequality by mixed spin-12 states: necessary and sufficient condition. Phys. Lett. A **200**, 340–344 (1995)
57. M.L. Hu, Relations between entanglement, Bell-inequality violation and teleportation fidelity for the two-qubit X states. Quantum Inf. Process **12**, 229–236 (2013)
58. S. Haddadi, M.A. Yurischev, M.Y. Abd-Rabbou, M. Azizi, M.R. Pourkarimi, M. Ghominejad, Quantumness near a Schwarzschild black hole. Eur. Phys. J. C **84**, 42 (2024)
59. M.A. Yurischev, S. Haddadi, Local quantum Fisher information and local quantum uncertainty for general X states. Phys. Lett. A **476**, 128868 (2023)
60. Z. Duan, M. Andronescu, K. Schutz, S. McIlwain, Y.J. Kim, C. Lee, W.S. Noble, A three-dimensional model of the yeast genome. Nature **465**, 363–367 (2010)